ACS OMEGA

Open Access



http://pubs.acs.org/journal/acsodf

Article

# Highly Green Fluorescent Carbon Dots from Gallic Acid: A Turn-On Sensor toward $Pb^{2+}$ Ions

Hardeep Kaur, Monika Bhattu, Subhendu Chakroborty, Manpreet Kaur Aulakh, Vishal Mutreja, Meenakshi Verma,* Karunesh Tiwari,* Chandra Chakraborty, and Ibrahim A. Darwish

Cite This: *ACS Omega* 2025, 10, 2354−2363

Read Online

ACCESS | Metrics & More | Article Recommendations

**ABSTRACT:** Carbon dots (CDs) are emerging novel fluorescent sensing nanomaterials owing to their tunable optical properties, biocompatibility, and eco-friendliness. Herein, we report a facile one-pot hydrothermal route for the synthesis of highly green fluorescent CDs using gallic acid (GA) as a single carbon source in *N*,*N*-dimethylformamide (DMF) solvent, which serves as a nitrogen source and reaction medium. The optical properties of the synthesized GA-DMF CDs were systematically characterized by using UV−vis and photoluminescence spectroscopy, revealing strong green fluorescence. Further, to gain insights into their size and structural, elemental, and chemical composition, Fourier transform infrared, dynamic light scattering, high-resolution transmission electron microscopy (HR-TEM), X-ray diffraction, and X-ray photoelectron spectroscopy characterization techniques were performed. HR-TEM analysis confirmed the formation of uniformly spherical GA-DMF CDs with an average particle size of 16 ± 6.1 nm. Notably, the GA-DMF CDs exhibited a highly selective and turn-on fluorescent response to $Pb^{2+}$ ions in aqueous solutions, which was attributed to a chelation-enhanced fluorescence mechanism. The detection limit for $Pb^{2+}$ ions was determined to be as low as $7.15 \times 10^{-7}$ M, with a broad linear detection range of 30−130 $\mu$M, underscoring their sensitivity and practical application in water quality monitoring. This study introduces a novel, sustainable approach for synthesizing nitrogen-doped CDs with outstanding optical properties and highlights their unprecedented selectivity toward $Pb^{2+}$ ions, advancing the development of efficient and eco-friendly sensing platforms for heavy metal detection.

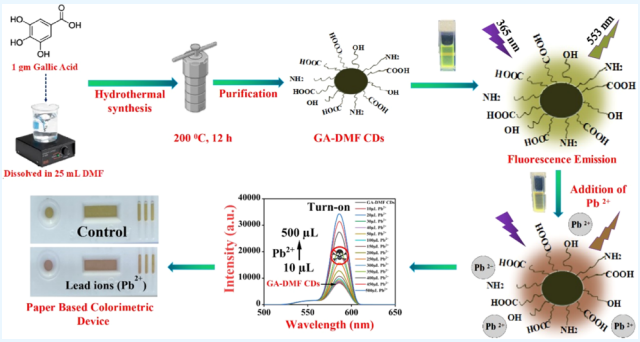


## 1. INTRODUCTION

Lead exposure has serious health consequences, especially for children, thus routine $Pb^{2+}$ detection in aquatic ecosystems continues to be of interest.[1] Although $Pb^{2+}$ is widely used in solar batteries and paint industries,[2] it is recognized as neurotoxic. It has been linked to chronic kidney and heart inflammation, impaired brain development, and decreased nerve conduction velocity.[3,4] The highest permitted lead concentration in drinking water as set by the US Environmental Protection Agency is 15 $\mu$g/L (about 72 nM). $Pb^{2+}$ detection techniques currently in use include atomic absorption spectrometry,[5] atomic fluorescence spectrometry,[6] inductively coupled plasma mass spectrometry,[7] and electrochemical stripping analysis.[8] Various attempts have also been performed to remove $Pb^{2+}$ from perovskite solar cells.[9] Although these methods provide low detection limits and accurate identification for $Pb^{2+}$, they are costly, complicated, time-consuming, and not appropriate for on-site field analysis. Several chemosensors have been developed to address the challenges associated with detecting $Pb^{2+}$ ions, including polymers,[10] semiconductor nanocrystals,[11] DNAzymes,[12] peptides,[13] proteins,[14] organic fluorophores, or chromophores.[15] Although colorimetric techniques are more appealing due to their lower apparatus costs and direct visual output, fluorescence-based detection methods still offer sensitivity and selectivity.[16] Fluorescence, however, is a necessary component of most known $Pb^{2+}$ chemosensors.[17] Among them, fluorescent carbon dots (CDs) are emerging fluorescent nanomaterials that are well-known for their optical and sensing potential toward heavy metals and other toxins. The preparation, characterization, and optical properties of CDs have been the subject of debate for a long time. For instance, different parameters facilitate the optical behavior of CDs, namely, (i)

**Received:** November 27, 2024
**Revised:** December 26, 2024
**Accepted:** December 31, 2024
**Published:** January 8, 2025

molecular byproducts during the synthesis[18,19] and (ii) intrinsic nature owing to surface defects.[20] The synthesis of CDs using green, sustainable precursors has gained significant attention due to growing concerns about environmental sustainability and the need to minimize the use of toxic chemicals in nanomaterial fabrication. Green precursors such as citric acid, glucose, plant extracts, and agricultural waste have been widely explored due to their abundance, low cost, and ability to produce CDs with diverse physicochemical properties. For example, biomass-derived sources such as rice husk, orange peel, and tea waste have been utilized for CD synthesis, offering a sustainable alternative to conventional chemical methods.[21] While these precursors offer several advantages, they also have limitations, including variable composition, inconsistent properties of the resulting CDs, and the need for additional purification steps.[22] In this study, gallic acid was selected as the precursor for synthesizing yellow fluorescent CDs. Gallic acid, a naturally occurring phenolic compound, offers several advantages over other green sources. Its high carbon content and the presence of hydroxyl groups facilitate efficient carbonization and functionalization, leading to CDs with well-defined optical properties. Additionally, gallic acid is relatively easy to handle and provides reproducible results compared to complex agricultural or biomass-derived precursors, which may require extensive preprocessing. The resulting CDs exhibited excellent photoluminescent properties, including strong yellow fluorescence, making them particularly suitable for environmental sensing applications. However, it is important to note some limitations of gallic acid. Compared with agricultural waste or other low-cost precursors, gallic acid may be relatively expensive and less scalable for large-scale applications. Despite this, its purity and consistent chemical composition make it an ideal choice for developing high-performance CDs with targeted applications. Further, investigating the structure of carbon dots from gallic acid could be a useful approach, as it would lead to a less complex reaction in comparison to other organic fluorophores.[12] For a single component, gallic acid has been in a couple of reports owing to a single reactive site.[23] On the other hand, solvents could also be significantly responsible for altering the structure and emission characteristics of carbon dots.[24,25] To date, different solvents such as ethanol, hexane, DCM, and dimethylformamide (DMF) are being used to produce multiple emissive CDs.[24,26−28] Various studies have verified the production of $sp^2$ domain CDs irrespective of solvents used during the reaction, which play an additional role of precursor. For instance, Heravi et al.[29] chose DMF as a reactant as well as a solvent for the solvothermal reaction. Furthermore, specific solvents may alter the reaction and can synthesize carbon dots with unique fluorescent properties.[25] In this direction, DMF has a distinctive ability to intervene in various organic transformations owing to its dual nature to behave as an electrophile or a nucleophile. DMF can be a part of many reactions and provides different types of building blocks, namely, $NMe_2$, $CONMe_2$, Me, CO, CHO, and many more. To illustrate, it has been observed that the DMF produces green emissive CDs via the solvothermal reaction.[27] Contrastingly, Qu et al.[30] revealed the synthesis of blue emissive CDs in a protic solvent such as water.

In the present article, we first prepared green-emitting GA-DMF CDs from gallic acid by a hydrothermal synthesis route employing DMF as the solvent system. Second, we investigate the wavelength-dependent emission behavior of prepared CDs with remarkable bathochromic shifts. We also present the turn-on sensing and selective capability of prepared CDs toward $Pb^{2+}$ metal ions.

## 2. MATERIALS AND METHODS

**2.1. Materials and Reagents.** Gallic acid and DMF were purchased from Sigma-Aldrich, and other solvents such as $H_2SO_4$, ethanol, quinine sulfate hexane, toluene, isopropanol, tetrahydrofuran (THF), ethyl acetate, dioxane, acetone, methanol, acetonitrile, and dimethyl sulfoxide (DMSO) were purchased from SRL chemicals. All reagents were used as such without further purification. Ultrapure water (Milli-Q water) was used in all experiments.

**2.2. Instrumentation.** UV−visible absorption spectroscopy was carried out by placing the CD solution in a 1 cm quartz cuvette and measuring using a Shimadzu UV-3600 UV−vis−NIR spectrophotometer at room temperature. Photoluminescence (PL) spectra were measured on a Hitachi F-7000 FL spectrophotometer at room temperature. FTIR spectra were measured on a Nicolet Avatar 360 FTIR spectrophotometer. Dynamic light scattering was performed on a Malvern Zetasizer. The high-resolution transmission electron microscopy (HR-TEM) images were recorded using a JEOL-2010 transmission electron microscope. X-ray diffraction (XRD) spectra of the powder samples were achieved on a Philips X-ray diffractometer with Cu K$\alpha$ radiation (l 1/4 1.541 °A).

**2.3. Synthesis of GA-DMF CDs.** First, 1.0 g of gallic acid was dissolved in 25 mL of DMF; then, the solution was transferred into a Teflon-lined stainless steel hydrothermal vessel. The solution was placed at 200 °C for 12 h in a muffle furnace and cooled to room temperature. The reaction mixture was centrifuged at 10 000 rpm for 20 min to remove high-weight precipitate and agglomerated particles. Further, the supernatant was filtered using a 0.22 $\mu$m syringe filter prior to being subjected to characterization and stored at 4 °C for further use. The synthetic method is represented in Figure 1.

**2.4. Quantum Yield Measurement.** The quantum yield of GA-DMF CDs was determined by the reference method[31] by using eq 1.

$$QY_{CDs} = QY_R \cdot \frac{grad_{CDs}}{grad_R} \cdot \frac{\eta^2_{CDs}}{\eta^2_R} \quad (1)$$

Here, QY represents the quantum yield, CDs represents the carbon dot sample solution whose quantum yield is to be calculated, subscript $R$ is the reference taken, which is quinine sulfate, and $\eta$ is the refractive index for the solvent used. The grad indicates the slope deduced from the linear curve between the integrated fluorescence intensity and UV−vis absorbance ($\lambda$ = 365 nm). The standard solution of quinine sulfate was acquired by dissolving quinine in 0.1 M $H_2SO_4$ at room temperature. The quantum yield for the quinine sulfate standard is 54% at 365 nm.

## 3. RESULTS AND DISCUSSION

**3.1. Optical Properties of GA-DMF CDs.** The optical properties of prepared GA-DMF CDs were determined using UV−vis and photoluminescence spectroscopic techniques (Figure 2). Figure 2a shows the presence of sharp and intense peaks at 270 and 300.5 nm, which could be ascribed to the $\pi-\pi^*$ transition of the aromatic $sp^2$ domains (C═C bonds) and $n-\pi^*$ transition, respectively.[32] The absorption band corresponds to the $n-\pi^*$ transition facilitating the fluorescent


https://doi.org/10.1021/acsomega.4c10796
ACS Omega 2025, 10, 2354−2363

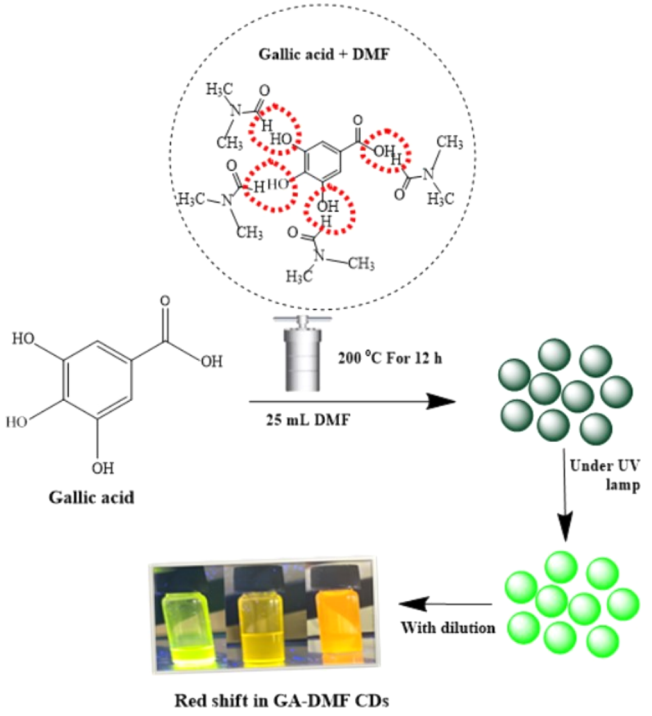


**Figure 1.** Schematic illustration of the preparation of green fluorescent GA-DMF CDs.

behavior of CDs.[32] Furthermore, the fluorescence property of prepared GA-DMF CDs was monitored over a wide range of wavelengths to identify the excitation dependency of emission properties (Figure 2b). The increase in excitation wavelength leads to a decrease in the intensity of emissive fluorescence intensity with a shift in excitation wavelength. The photoluminescence spectrum of GA-DMF CDs exhibits a prominent emission peak at 553 nm, which corresponds to their observed green fluorescence and reflects the presence of C/N groups on CDs' surface.[33,34]

**3.2. FTIR Spectroscopic Characterization.** To gauge the presence of functional groups in both GA-CDs and GA-DMF CDs, FTIR spectroscopic analysis was performed (Figure 3). The spectrum of GA-CDs shows a strong, broad peak at 3297 $cm^{-1}$ owing to a −OH stretching vibrations.[35] On the other side, the weak broad peak at 3488.2 $cm^{-1}$ is due to the stretching of −NH and OH bonds, suggesting that abundant hydroxyl and amine groups bonded on the surface of GA-DMF

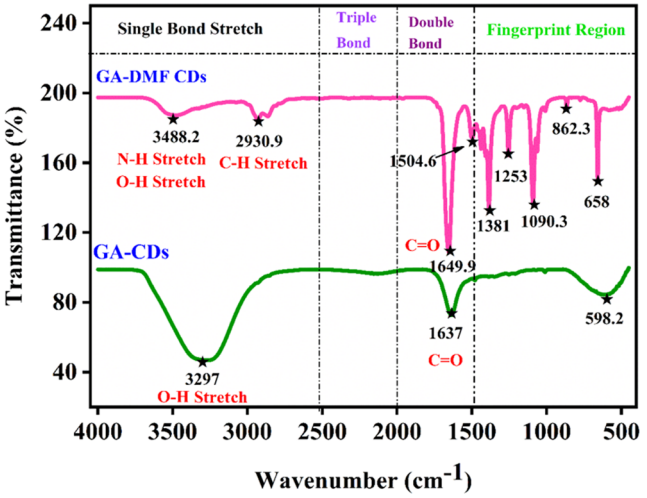


**Figure 3.** FTIR analysis of GA-CDs and GA-DMF CDs.

CDs.[36,37] Peak values at 1649.9 and 1637 $cm^{-1}$ in both nanomaterials are assigned to C═C and C═O stretching vibrations. The peaks near the fingerprint region such as 1381, 1253, and 1090.3 $cm^{-1}$ are due to the stretching frequencies of C−N and C−O−C bonds.[23] The presence of different functional moieties on the surface of CDs imparts a hydrophilic nature to the carbon dots and increases their aqueous solubility.[32,38]

**3.3. XRD of GA-DMF CDs and GA-CDs.** The crystalline properties of the prepared GA-CDs and GA-DMF CDs were investigated by using XRD analysis. The XRD pattern (Figure 4a) revealed a wide peak at $2\theta = 23.5°$, attributed to the (002) plane of graphitic carbon, indicating the material's amorphous characteristics.[37,39] The peak's width confirms the $sp^2$ hybridization characteristic of amorphous carbon in GA-DMF CDs, aligning with previous studies.[40] Similar findings were reported by Bora et al.[32] for blue-emitting CDs produced from gallic acid and DMF, showing a diffraction peak near $2\theta = 23°$. For comparison purposes, carbon dots derived from gallic acid using water as the solvent were also examined. These CDs exhibited a broad XRD peak at $2\theta = 24.5°$ (Figure 4b), also demonstrating an amorphous structure with predominant $sp^2$-hybridized carbon. The difference in peak positions between GA-DMF CDs and water-based CDs indicates the solvent's role in determining carbon arrangement within the CDs. XRD data reveal that GA-DMF CDs ($2\theta = 23.5°$) possess a more

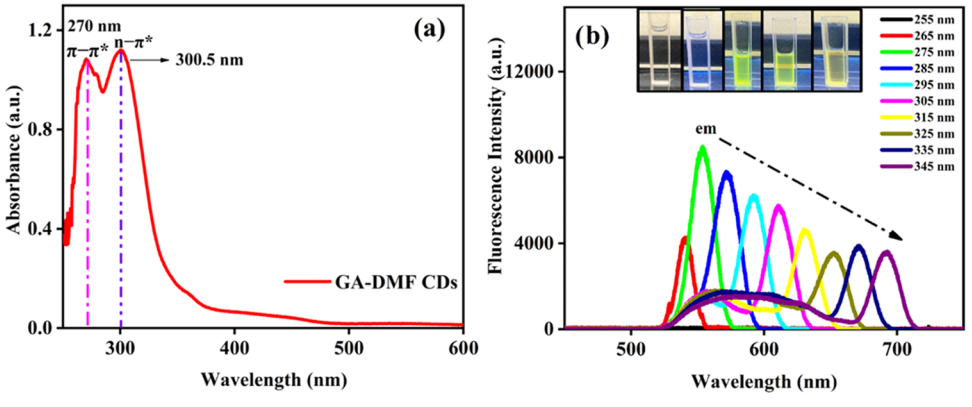


**Figure 2.** (a) UV−vis spectra of the GA-DMF CDs. (b) PL spectra of GA-DMF CDs at different excitation wavelengths (255−345 nm).



https://doi.org/10.1021/acsomega.4c10796
ACS Omega 2025, 10, 2354−2363

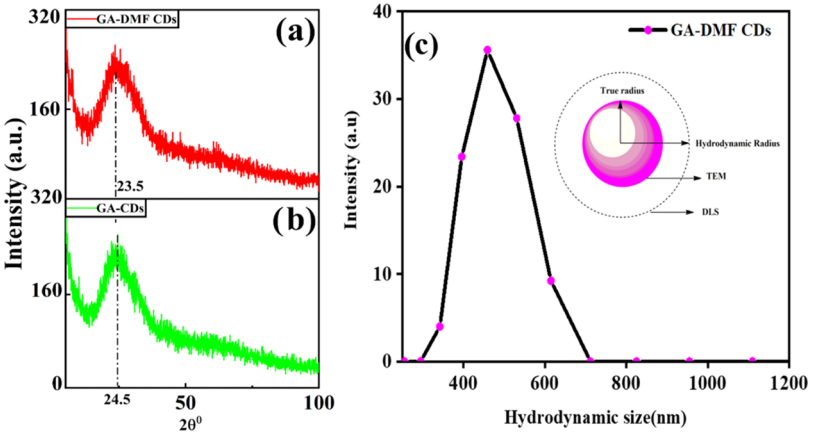


**Figure 4.** (a) XRD of GA-DMF CDs. (b) XRD of GA-CDs. (c) DLS of the GA-DMF CDs.

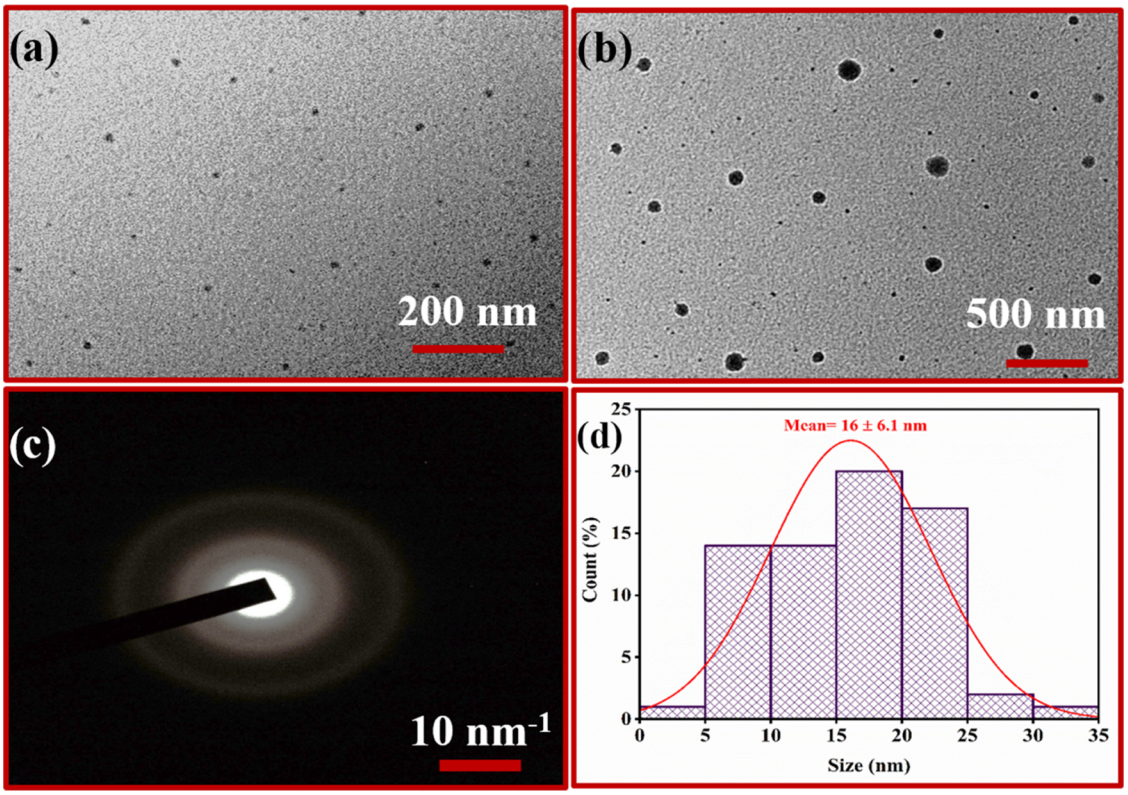


**Figure 5.** (a, b) HR-TEM, (c) SAED pattern, and (d) histogram of the particle size distribution for GA-DMF CDs.

consistent graphitic carbon framework than water-based CDs ($2\theta$ = 24.5°). Furthermore, DMF facilitates nitrogen incorporation, as shown by improved optical characteristics, making it preferable for applications requiring strong fluorescence performance and structural stability.[41]

**3.4. DLS of GA-DMF CDs.** The particle size of the synthesized GA-DMF CDs was also examined by DLS. The average hydrodynamic particle size of synthesized GA-DMF CDs was found to be approximately 458 nm (Figure 4c). Owing to the presence of the hydrophilic functional groups on the surface of the CDs, the larger hydrodynamic size of GA-DMF CDs was observed, indicating possible aggregation in the suspension.

**3.5. HR-TEM.** Additionally, to analyze the insight into the morphology and size of synthesized GA-DMF CDs, HR-TEM analysis was performed. The HR-TEM images display spherical nanoparticle formation of deposited solution on the grid with an average diameter of 16 ± 6.1 nm (Figure 5a–d). Literature reveals that organic fluorophores normally form amorphous aggregates.[23] Expectedly, no lattice fringes were observed in the selected area electron diffraction (SAED) pattern of the product (Figure 5c). These results are in good correlation with the information obtained from the XRD pattern of GA-DMF CDs. In the same direction, Pal et al.[23] reported yellow-emissive CDs obtained from gallic and dry DMF solvent via solvothermal treatment at 160 °C for 24 h. The particle average size of the obtained CDs was found to be 5.4 ± 0.7 nm. On the other hand, Zheng et al.[42] introduced the synthesis of green emissive gallic acid-based CDs having particle size range from 20 to 30 nm in the presence of polyene polyamine via solvothermal treatment of 180 °C for 6 h.



https://doi.org/10.1021/acsomega.4c10796
ACS Omega 2025, 10, 2354−2363

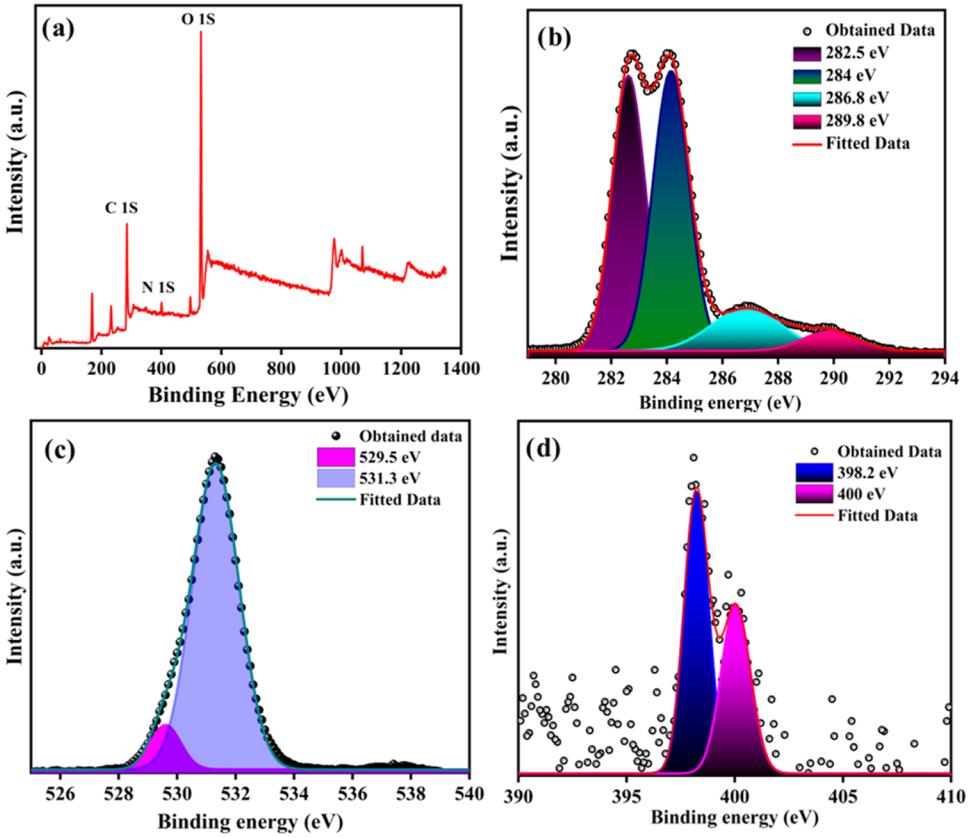


**Figure 6.** (a) Full-scan XPS spectrum of GA-DMF CDs. (b) High-resolution XPS spectrum of C 1s. (d) The high-resolution XPS spectrum of N 1s. (d) The high-resolution XPS spectrum of O 1s.

**3.6. XPS.** To investigate the composition and oxidation state of the elements present in the GA-DMF CDs, XPS analysis was carried out. The full-scan spectrum of prepared GA-DMF CDs (Figure 6a) showed three major peaks at 532, 400, and 284 eV, which correspond to O 1s, N 1s, and C 1s, respectively. The high-resolution scan of the C 1s region on deconvolution showed the presence of carbon in three different chemical environments (Figure 6b) at 284, 286.8, and 289.8 eV corresponding to C═C, C−O/C−N, and O−C═O, respectively. The high-resolution scan of the O 1s region was deconvoluted into two peaks at 529.5 and 531.3 eV (Figure 6c), corresponding to the −C═O and −C−O bonds,[23,43] respectively. The N 1s spectrum was further deconvoluted into two peaks at 398.2 and 400 eV (Figure 6d), attributed to C−N and N−H groups, respectively,[43] which are in correspondence with the already reported literature.[43−49]

Similarly, the full-scan XPS spectrum of GA-CDs showed two peaks at 285 and 532 eV corresponding to C 1s and O 1s, respectively (Figure 7a.). The peak in the C 1s spectrum (Figure 7b) was deconvoluted into four peaks at binding energies of 284.1, 285.6, 288.2, and 292.1 eV, indicating the existence of C═O, C−O, and C−H structures in the prepared CDs. The O 1s spectrum exhibited two peaks (Figure 7d) at 529.9, 531.2, and 531.6 eV, attributed to −OH and C═O bonds.

Thus, the preparation of CDs in DMF illustrates an additional nitrogen peak owing to the participation of the amide group in CD formation, which confirms the formation of N-doped CDs.

**3.7. Selective and Sensitive Sensing of $Pb^{2+}$ Ions.** To elucidate the sensing potential of GA-DMF CDs toward metal toxins, a photoluminescence analysis was performed in which, initially, the prepared CDs were screened against different metal ions, including $Fe^{2+}$, $Fe^{3+}$, $Ni^{2+}$, $Co^{2+}$, $Zn^{2+}$, $Cd^{2+}$, $Hg^{2+}$, $Mn^{2+}$, $Cu^{2+}$, $K^{+}$, and $Pb^{2+}$ ions. For this investigation, 100 $\mu$L of 1 mM solutions of different metal ions were mixed with a sensing solution of GA-DMF CDs, and the change in the fluorescence response was monitored. All of the metal ions did not exhibit any considerable change except $Pb^{2+}$, which exhibits an intense turn-on behavior, which is evident for some kinds of interaction between GA-DMF CDs and Pb (Figure 8a,b). Further, titration studies were performed to find the sensitivity and binding affinity of GA-DMF CDs toward $Pb^{2+}$. It is observed from Figure 8c that on the sequential addition of $Pb^{2+}$ ions from 10 to 500 $\mu$L, a steady increase in the fluorescence intensity of GA-DMF CDs was observed. On the addition of 500 $\mu$L of $Pb^{2+}$ ions, an approximately 4-fold increase was noticed, which became saturated on further additions.

Further, the change in the normalized fluorescence signal with the change in the concentration of the $Pb^{2+}$ ion is shown in Figure 8d. Additionally, the limit of detection was determined by applying the given equation.

$$\mathrm{LOD} = 3\sigma/s$$

In the above equation, "$\sigma$" is the standard deviation, and "s" is related to the slope of the calibration curve. The limit of detection for the $Pb^{2+}$ ion was estimated at $7.15 \times 10^{-4}$ M with a linear range from 30 to 120 $\mu$M.

Along with this, an anti-interference experiment was also performed to find out the specific selectivity of GA-DMF CDs toward $Pb^{2+}$ ions in the presence of other interfering metal ions


https://doi.org/10.1021/acsomega.4c10796
ACS Omega 2025, 10, 2354−2363

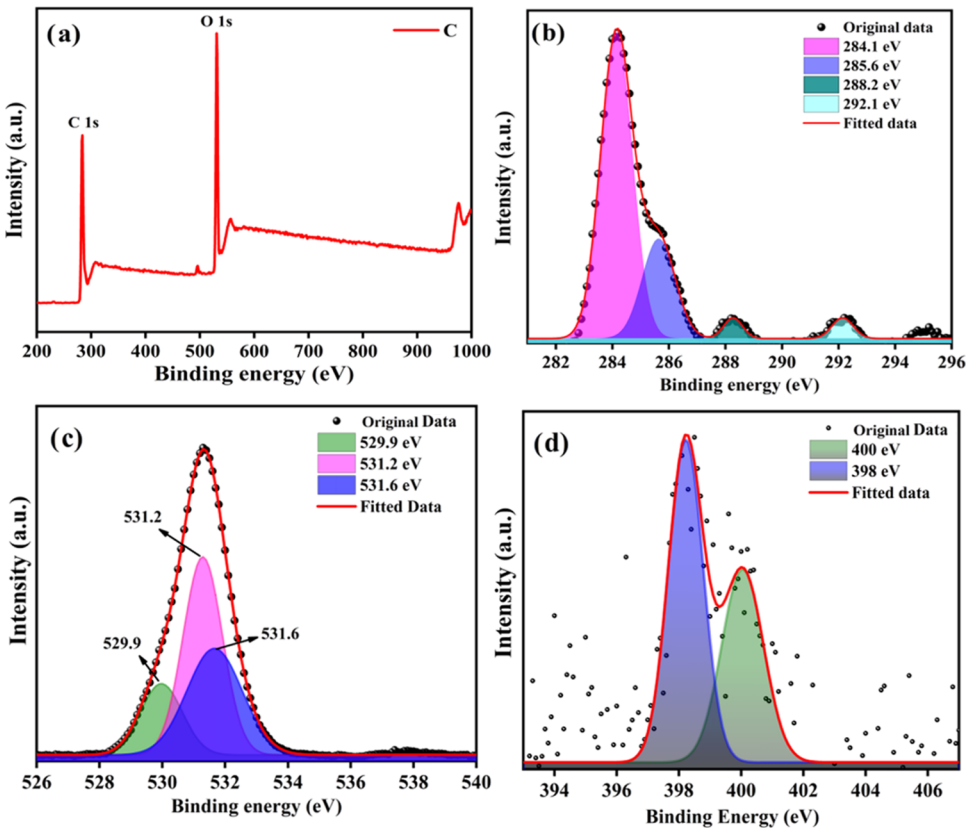


**Figure 7.** (a) Full-scan XPS spectrum of GA-CDs. (b) The high-resolution XPS spectrum of C 1s. (c) The high-resolution XPS spectrum of N 1s. (d) The high-resolution XPS spectrum of O 1s.

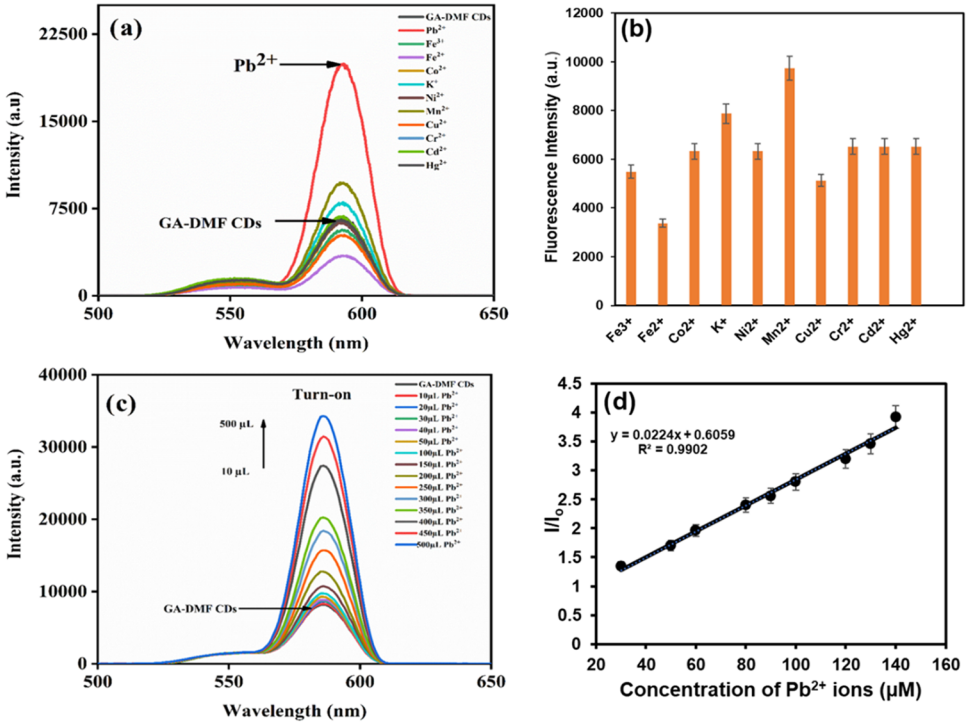


**Figure 8.** (a) Fluorescence study of different metal ion detection using GA-DMF CDs. (b) Comparative selectivity of GA-DMF CDs toward different metal ions. (c) Fluorescence spectra of GA-DMF CDs upon addition of various concentrations of $Pb^{2+}$ metal ions from 10 to 500 $\mu$L. (d) LOD calculation for GA-DMF CDs against $Pb^{2+}$ ions.

such as $Fe^{2+}$, $Fe^{3+}$, $Ni^{2+}$, $Co^{2+}$, $Zn^{2+}$, $Cd^{2+}$, $Hg^{2+}$, $Mn^{2+}$, $Cu^{2+}$, and $K^{+}$ (Figure 9). It was observed that the fluorescence intensity of the sensor toward $Pb^{2+}$ was not significantly altered in the presence of other coexisting metal ions. Hence,



https://doi.org/10.1021/acsomega.4c10796
ACS Omega 2025, 10, 2354−2363

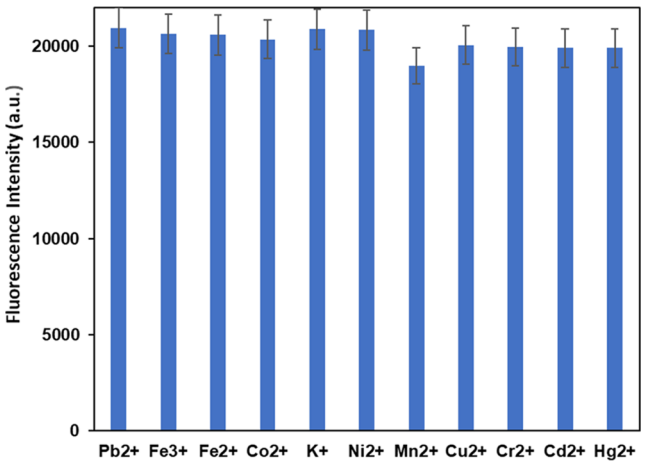


**Figure 9.** Interference study of GA-DMF CDs against $Pb^{2+}$ ions in the presence of different metal ions such as $Fe^{2+}$, $Fe^{3+}$, $Ni^{2+}$, $Co^{2+}$, $Zn^{2+}$, $Cd^{2+}$, $Hg^{2+}$, $Mn^{2+}$, $Cu^{2+}$, and $K^{+}$.

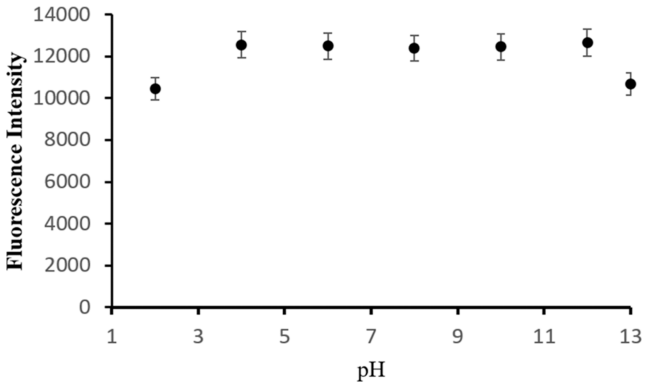


**Figure 10.** Illustration of the effect of pH on the complex of CDs + $Pb^{2+}$.

fluorescence sensing studies strongly prove that the GA-DMF CDs possess high selectivity toward the detection of $Pb^{2+}$ ions (Table 1) (Figure 10).

Furthermore, the effect of pH has also been studied on the metal complex by varying the pH by adding 0.1 N NaOH and 0.1 M HCl to make the solution basic and acidic, respectively. The complex was found to be stable over a pH range of 4−12, which signifies the high sensitivity of the probe for the detection of $Pb^{2+}$.

**3.8. Mechanism of the Turn-On Signal.** To get in-depth insights into the sensing mechanism and reaction, the same reaction conditions were provided to different salts of lead in +2 oxidation states and GA-DMF CDs, as in the case of lead chloride. Further, UV−visible, FTIR, and fluorescence spectra of all samples were recorded (Figure 11a−c). It has been observed that the UV−visible spectra of all reaction mixtures displayed a red shift of more than 10 nm, which is possibly due to the formation of a chelating complex or salt. The ionic radius and charge density of the $Pb^{2+}$ ion highly favor the interaction of metal ions with oxygen-containing functional groups of CDs. Second, the involvement of a common reaction mechanism in all reaction mixtures is strengthened by the finding of similarity in the range of 1500−700 $cm^{-1}$ of the FTIR spectra (Figure 11c). The emergence of hydroxyl group peaks on the addition of Pb(II) suggests the participation of the hydroxyl group in bond formation and leads to a detectable peak in FTIR spectra. Additionally, the new band in the range of 400−600 $cm^{-1}$ signifies the formation of the Pb−O bond. Moreover, the interference studies showed the selective interaction of ions with CDs, which has been proven experimentally (Figure 9). Lastly, the enhancement in the FL intensity was observed in all different salts interacting with GA-DMF CDs in the +2 oxidation state (Figure 11b). However, the turn-on signal in FL spectra in the presence of heavy metals is mainly due to chelation-enhanced fluorescence[50] and aggregation-induced emission enhancement.[51] Based on the above observations, we propose that the reaction mechanism associated with the sensing of Pb(II) ions could be due to the chelate formation between Pb(III) ions and GA-DMF CDs (Figure 11d).

## 4. PAPER-BASED COLORIMETRIC DEVICE FOR $PB^{2+}$ ION SENSING

To demonstrate the colorimetric response of GA-DMF CDs toward $Pb^{2+}$ metal ions, we immobilized the GA-DMF CDs on the Whatman filter paper of grade 1 (Figure 12(a−d)). Further, we put an analyte sample, i.e., $Pb^{2+}$ ions, on the detection zone. After the addition of the analyte, vigorously, we observed the color change from pale yellow to baby light pink color. Along with the colorimetric response of GA-DMF CDs against lead ions, we also observed a similar change under UV radiation, as shown in Figure 13. The paper strip immobilized with GA-DMF CDs (hydrophilic) is fixed in a plastic case with different parts. The first part is the sample hole, where we drop-cast our analyte, and the sample will follow a microfluidic channel flow into the detection part and will display the instance color change.

Furthermore, the intensity of color goes on increasing, increasing the concentration of the $Pb^{2+}$ solution, which illustrates the quantification of the metal ion in real samples. In this regard, different kinds of water samples, including tap water, RO water, and distilled water, were initially analyzed for the $Pb^{2+}$ ion and further spiked with a known concentration of ions varying from 25 to 100 nM. The probe showed a recovery of 98−100% in the spiked samples, which signifies CDs as a potential and most efficient sensor for the quantification of $Pb^{2+}$ in different water samples.

**Table 1. Comparison of Sensing Parameters of Our Sensing Probe for $Pb^{2+}$ with Those Reported in the Literature**

| sr. no. | material used | treatment | type of signal | mechanism | LOD | ref |
|---|---|---|---|---|---|---|
| 1. | chocolate | hydrothermal | turn-off | complex formation | 12.7 nM | 52 |
| 2. | sodium citrate and polyacrylamide | hydrothermal | turn-off | complex formation | 4.6 nM | 53 |
| 3. | L-lysine and L-glutathione | hydrothermal | turn-off | complex formation | 2.2 $\mu$M | 54 |
| 4. | pearl millet seeds | hydrothermal | turn-on | complex formation | 0.18 nM | 55 |
| 5. | gallic and DMF | hydrothermal | turn-on | complex formation | $7.15 \times 10^{-4}$ M | this study |



https://doi.org/10.1021/acsomega.4c10796
ACS Omega 2025, 10, 2354−2363

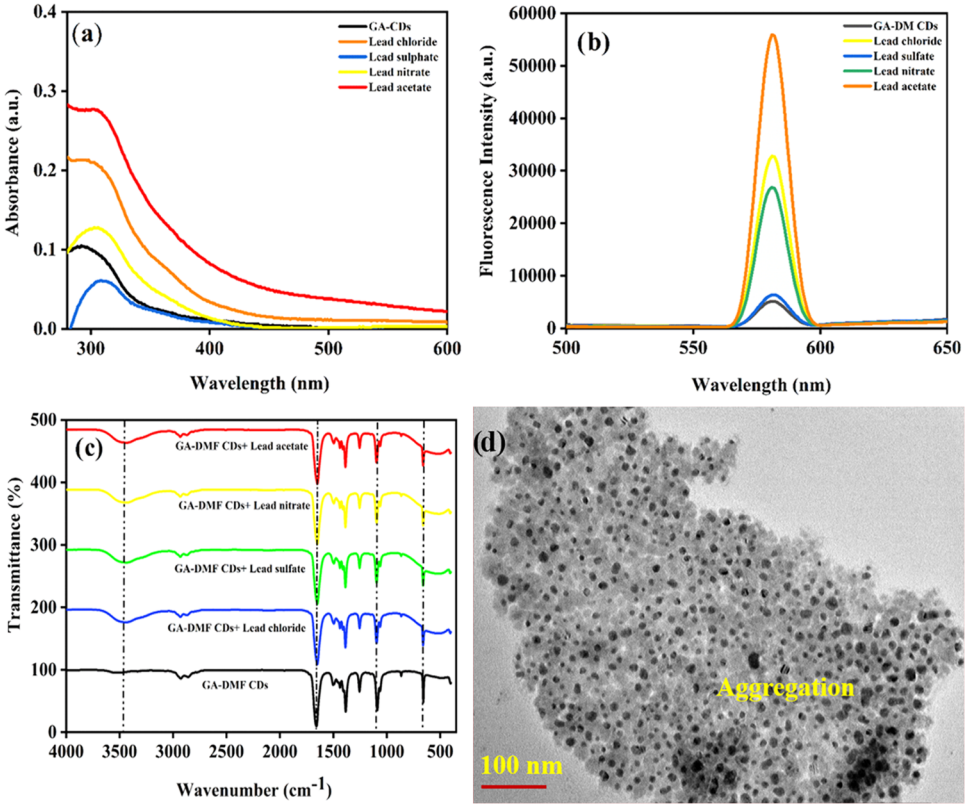


**Figure 11.** (a) UV−visible spectra of reaction mixtures of GA-DMF CDs and $Pb^{2+}$ metal in different salts. (b) Fluorescence spectra of reaction mixtures of GA-DMF CDs and $Pb^{2+}$ metal in different salts. (c) FTIR spectra of reaction mixtures of GA-DMF CDs and $Pb^{2+}$ metal in different salts. (d) Aggregation of particles after the addition of $Pb^{2+}$ metal into GA-DMF CDs.

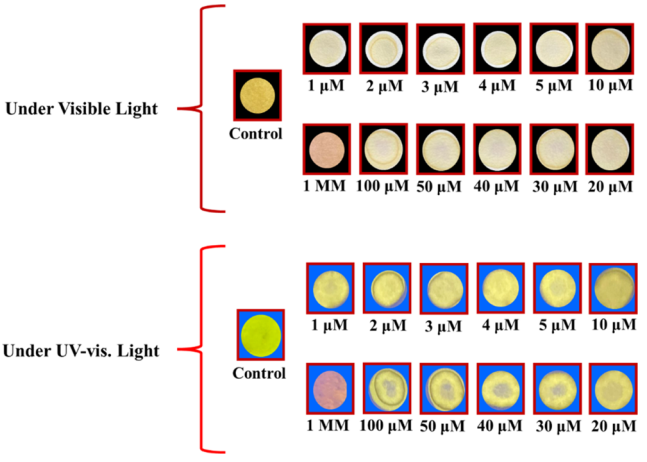


**Figure 12.** (a, b) Colorimetric response of GA-DMF CDs toward $Pb^{2+}$ on Whatman filter paper. (c, d) Fluorimetric response of GA-DMF CDs toward $Pb^{2+}$ on Whatman filter paper.

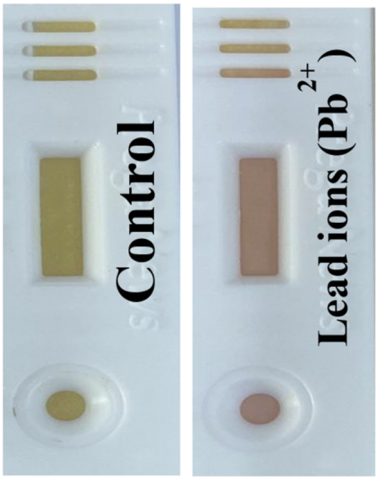


**Figure 13.** Paper-based colorimetric device for $Pb^{2+}$ metal ions.

## 5. CONCLUSIONS AND FUTURE ASPECTS

In summary, hydrophilic green fluorescent CDs were prepared by a one-pot hydrothermal synthesis route from pure gallic acid in the DMF solvent. The prepared CDs indicated turn-on signals in emission spectra to detect lead ions. The prepared sensor exhibits a fluorescence turn-on response toward the detection of $Pb^{2+}$. Based on the aggregation-induced emission enhancement mechanism, the results revealed that the GA-DMF CDs-based fluorescent sensor had the advantages of high selectivity, sensitivity, low cost, and the absence of any other chemical surface modifications. The limit of detection for $Pb^{2+}$ was calculated to be $7.15 \times 10^{-4}$ M under optimized conditions, and the linear response was observed over a concentration range of 30−120 $\mu$M. The developed method upholds the potential sensing efficacy for the detection of lead in the environmental and biological field.

## ■ ASSOCIATED CONTENT

### Data Availability Statement

The authors declare that the data supporting the findings of this study are available within the paper and its Supporting Information file.



https://doi.org/10.1021/acsomega.4c10796
ACS Omega 2025, 10, 2354−2363

## AUTHOR INFORMATION


### Corresponding Authors

**Karunesh Tiwari** − *Department of Physics, Mai Nefhi College of Science, Eritrean Institute of Technology, Mai Nefhi 6QVF +4WV Maekel Region, Eritrea;* orcid.org/0000-0002-4119-5727; Email: tdrkarunesh@gmail.com

**Meenakshi Verma** − *University Centre for Research and Development, Chandigarh University, Mohali 140 413 Punjab, India*; Email: meenakshi.j3505@cgc.ac.in

### Authors

**Hardeep Kaur** − *Department of Biotechnology, University Institute of Biotechnology, Chandigarh University, Mohali 140 413 Punjab, India*

**Monika Bhattu** − *Department of Chemistry, Research and Incubation Centre, Rayat Bahra University, Greater Mohali 140103 Punjab, India; Centre of Research Impact and Outcome, Chitkara University, Rajpura 140417 Punjab, India*

**Subhendu Chakroborty** − *School of Applied Sciences, Chandigarh University, Unnao 209859 Uttar Pradesh, India*

**Manpreet Kaur Aulakh** − *Department of Chemistry, University Institute of Sciences, Chandigarh University, Mohali 140 413 Punjab, India*

**Vishal Mutreja** − *Department of Chemistry, University Institute of Sciences, Chandigarh University, Mohali 140 413 Punjab, India*

**Chandra Chakraborty** − *Department of Allied Sciences, Graphic Era (Deemed to be University), 248002 Dehradun, India*

**Ibrahim A. Darwish** − *Department of Pharmaceutical Chemistry, College of Pharmacy, King Saud University, Riyadh 11451, Saudi Arabia*

Complete contact information is available at: https://pubs.acs.org/10.1021/acsomega.4c10796


### Notes

The authors declare no competing financial interest.

## ACKNOWLEDGMENTS

H.K. and M.V. are thankful to DST (File No: DST/WOS-B/WWM-9/2021). The authors would like to extend their appreciation to the Researchers Supporting Project Number (RSPD2025R944), King Saud University, Riyadh, Saudi Arabia, for funding this work.

## REFERENCES


(1) Sanders, T.; Liu, Y.; Buchner, V.; Tchounwou, P. B. Neurotoxic Effects and Biomarkers of Lead Exposure: A Review. *Rev. Environ. Health* **2009**, *24* (1), 15−46, DOI: 10.1515/REVEH.2009.24.1.15.

(2) Liu, K.; Hu, T.; Cai, Z.; Liu, F.; Rafique, S.; Li, X.; Deng, L.; Li, C.; Wang, Y.; Guo, Q.; et al. Lead (Pb) Management in the Entire Life Cycle of Highly Efficient and Stable Perovskite Solar Cells. *Energy Environ. Sci.* **2024**, *17* (15), 5576−5587.

(3) Schroeder, H. A.; Tipton, I. H. The Human Body Burden of Lead. *Arch. Environ. Health: Int. J.* **1968**, *17* (6), 965−978.

(4) Araki, S.; Sato, H.; Yokoyama, K.; Murata, K. Subclinical Neurophysiological Effects of Lead: A Review on Peripheral, Central, and Autonomic Nervous System Effects in Lead Workers. *Am. J. Ind. Med.* **2000**, *37* (2), 193−204.

(5) Yang, L.; Saavedra, S. S. Chemical Sensing Using Sol-Gel Derived Planar Waveguides and Indicator Phases. *Anal. Chem.* **1995**, *67* (8), 1307−1314.

(6) Wagner, E. P.; Smith, B. W.; Winefordner, J. D. Ultratrace Determination of Lead in Whole Blood Using Electrothermal Atomization Laser-Excited Atomic Fluorescence Spectrometry. *Anal. Chem.* **1996**, *68* (18), 3199−3203.

(7) Bowins, R. J.; McNutt, R. H. Electrothermal Isotope Dilution Inductively Coupled Plasma Mass Spectrometry Method for the Determination of Sub-Ng Ml−1 Levels of Lead in Human Plasma. *J. Anal. At. Spectrom.* **1994**, *9* (11), 1233−1236.

(8) Feldman, B. J.; Osterloh, J. D.; Hata, B. H.; D'Alessandro, A. Determination of Lead in Blood by Square Wave Anodic Stripping Voltammetry at a Carbon Disk Ultramicroelectrode. *Anal. Chem.* **1994**, *66* (13), 1983−1987.

(9) Mehrabian, M.; Akhavan, O.; Rabiee, N.; Afshar, E. N.; Zare, E. N. Lead-Free MAGeI3 as a Suitable Alternative for MAPbI3 in Nanostructured Perovskite Solar Cells: A Simulation Study. *Environ. Sci. Pollut. Res.* **2023**, *30*, 57032−57040.

(10) Reese, C. E.; Baltusavich, M. E.; Keim, J. P.; Asher, S. A. Development of an Intelligent Polymerized Crystalline Colloidal Array Colorimetric Reagent. *Anal. Chem.* **2001**, *73* (21), 5038−5042.

(11) Mohamed Ali, E.; Zheng, Y.; Yu, H.; Ying, J. Y. Ultrasensitive Pb2+ Detection by Glutathione-Capped Quantum Dots. *Anal. Chem.* **2007**, *79* (24), 9452−9458.

(12) Huang, K.-W.; Yu, C.-J.; Tseng, W.-L. Sensitivity Enhancement in the Colorimetric Detection of Lead (II) Ion Using Gallic Acid−Capped Gold Nanoparticles: Improving Size Distribution and Minimizing Interparticle Repulsion. *Biosens. Bioelectron.* **2010**, *25* (5), 984−989.

(13) Deo, S.; Godwin, H. A. A Selective, Ratiometric Fluorescent Sensor for Pb2+. *J. Am. Chem. Soc.* **2000**, *122* (1), 174−175.

(14) Chen, P.; Greenberg, B.; Taghavi, S.; Romano, C.; van der Lelie, D.; He, C. An Exceptionally Selective Lead (II)-regulatory Protein from Ralstonia Metallidurans: Development of a Fluorescent Lead (II) Probe. *Angew. Chem.* **2005**, *117* (18), 2775−2779.

(15) Ranyuk, E.; Douaihy, C. M.; Bessmertnykh, A.; Denat, F.; Averin, A.; Beletskaya, I.; Guilard, R. Diaminoanthraquinone-Linked Polyazamacrocycles: Efficient and Simple Colorimetric Sensor for Lead Ion in Aqueous Solution. *Org. Lett.* **2009**, *11* (4), 987−990.

(16) Zare, H.; Ghalkhani, M.; Akhavan, O.; Taghavinia, N.; Marandi, M. Highly Sensitive Selective Sensing of Nickel Ions Using Repeatable Fluorescence Quenching-Emerging of the CdTe Quantum Dots. *Mater. Res. Bull.* **2017**, *95*, 532−538.

(17) He, Q.; Miller, E. W.; Wong, A. P.; Chang, C. J. A Selective Fluorescent Sensor for Detecting Lead in Living Cells. *J. Am. Chem. Soc.* **2006**, *128* (29), 9316−9317.

(18) Essner, J. B.; Kist, J. A.; Polo-Parada, L.; Baker, G. A. Artifacts and Errors Associated with the Ubiquitous Presence of Fluorescent Impurities in Carbon Nanodots. *Chem. Mater.* **2018**, *30* (6), 1878−1887.

(19) Mishra, K.; Koley, S.; Ghosh, S. Ground-State Heterogeneity along with Fluorescent Byproducts Causes Excitation-Dependent Fluorescence and Time-Dependent Spectral Migration in Citric Acid-Derived Carbon Dots. *J. Phys. Chem. Lett.* **2019**, *10* (3), 335−345.

(20) Kong, W.; Wu, H.; Ye, Z.; Li, R.; Xu, T.; Zhang, B. Optical Properties of PH-Sensitive Carbon-Dots with Different Modifications. *J. Lumin.* **2014**, *148*, 238−242.

(21) Tayyebi, A.; Akhavan, O.; Lee, B.-K.; Outokesh, M. Supercritical Water in Top-down Formation of Tunable-Sized Graphene Quantum Dots Applicable in Effective Photothermal Treatments of Tissues. *Carbon* **2018**, *130*, 267−272.

(22) El-Reash, Y. G. A.; Ghaith, E. A.; El-Awady, O.; Algethami, F. K.; Lin, H.; Abdelrahman, E. A.; Awad, F. S. Highly Fluorescent Hydroxyl Groups Functionalized Graphitic Carbon Nitride for Ultrasensitive and Selective Determination of Mercury Ions in Water and Fish Samples. *J. Anal. Sci. Technol.* **2023**, *14* (1), 16.

(23) Pal, S. K.; Parashar, M.; Kanrar, B. B.; Panda, S.; Roy, N.; Paira, P.; Panda, D. N-Doped Yellow-Emissive Carbon Nanodots from Gallic Acid: Reaction Engineering, Stimuli-Responsive Red Emission, and Intracellular Localization. *J. Phys. Chem. C* **2021**, *125* (10), 5748−5759.

(24) Huo, X.; Shen, H.; Liu, R.; Shao, J. Solvent Effects on Fluorescence Properties of Carbon Dots: Implications for Multicolor Imaging. *ACS Omega* **2021**, *6* (40), 26499−26508.
(25) Kumari, R.; Sahu, S. K. Effect of Solvent-Derived Highly Luminescent Multicolor Carbon Dots for White-Light-Emitting Diodes and Water Detection. *Langmuir* **2020**, *36* (19), 5287−5295.
(26) Chen, M.; Liu, C.; An, Y.; Li, Y.; Zheng, Y.; Tian, H.; Shi, R.; He, X.; Lin, X. Red, Green, and Blue Light-Emitting Carbon Dots Prepared from Gallic Acid for White Light-Emitting Diode Applications. *Nanoscale Adv.* **2021**, *4* (1), 14−18.
(27) Du, Q.; Zheng, J.; Wang, J.; Yang, Y.; Liu, X. The Synthesis of Green Fluorescent Carbon Dots for Warm White LEDs. *RSC Adv.* **2018**, *8* (35), 19585−19595.
(28) Yang, M.; Li, B.; Zhong, K.; Lu, Y. Photoluminescence Properties of N-Doped Carbon Dots Prepared in Different Solvents and Applications in PH Sensing. *J. Mater. Sci.* **2018**, *53* (4), 2424−2433.
(29) Heravi, M. M.; Ghavidel, M.; Mohammadkhani, L. Beyond a Solvent: Triple Roles of Dimethylformamide in Organic Chemistry. *RSC Adv.* **2018**, *8* (49), 27832−27862.
(30) Qu, D.; Zheng, M.; Li, J.; Xie, Z.; Sun, Z. Tailoring Color Emissions from N-Doped Graphene Quantum Dots for Bioimaging Applications. *Light: Sci. Appl.* **2015**, *4* (12), e364 DOI: 10.1038/LSA.2015.137.
(31) Lv, R.; Li, G.; Lu, S.; Wang, T. Synthesis of Multi-Functional Carbon Quantum Dots for Targeted Antitumor Therapy. *J. Fluoresc.* **2021**, *31* (2), 339−348.
(32) Bora, A.; Mohan, K.; Dolui, S. K. Carbon Dots as Cosensitizers in Dye-Sensitized Solar Cells and Fluorescence Chemosensors for 2,4,6-Trinitrophenol Detection. *Ind. Eng. Chem. Res.* **2019**, *58* (51), 22771−22778.
(33) Wang, T.; Chen, G.; Li, L.; Wu, Y. Highly Fluorescent Green Carbon Dots as a Fluorescent Probe for Detecting Mineral Water PH. *Sensors* **2019**, *19* (17), 3801.
(34) Wang, H.; Sun, C.; Chen, X.; Zhang, Y.; Colvin, V. L.; Rice, Q.; Seo, J.; Feng, S.; Wang, S.; William, W. Y. Excitation Wavelength Independent Visible Color Emission of Carbon Dots. *Nanoscale* **2017**, *9* (5), 1909−1915.
(35) Wang, H.; Zhang, T.; Zhu, J.; Zhai, Y.; Wang, H.; Bai, X.; Dong, B.; Song, H. A Novel Mechanism for Red Emission Carbon Dots: Hydrogen Bond Dominated Molecular States Emission. *Nanoscale* **2017**, *9* (35), 13042−13051.
(36) Lu, S.; Liu, L.; Wang, H.; Zhao, W.; Li, Z.; Qu, Z.; Li, J.; Sun, T.; Wang, T.; Sui, G. Synthesis of Dual Functional Gallic-Acid-Based Carbon Dots for Bioimaging and Antitumor Therapy. *Biomater. Sci.* **2019**, *7* (8), 3258−3265.
(37) Kitchawengkul, N.; Prakobkij, A.; Anutrasakda, W.; Yodsin, N.; Jungsuttiwong, S.; Chunta, S.; Amatatongchai, M.; Jarujamrus, P. Mimicking Peroxidase-Like Activity of Nitrogen-Doped Carbon Dots (N-CDs) Coupled with a Laminated Three-Dimensional Microfluidic Paper-Based Analytical Device (Laminated 3D-MPAD) for Smart Sensing of Total Cholesterol from Whole Blood. *Anal. Chem.* **2021**, *93* (18), 6989−6999.
(38) Xu, X.; Cai, L.; Hu, G.; Mo, L.; Zheng, Y.; Hu, C.; Lei, B.; Zhang, X.; Liu, Y.; Zhuang, J. Red-Emissive Carbon Dots from Spinach: Characterization and Application in Visual Detection of Time. *J. Lumin.* **2020**, *227*, No. 117534.
(39) Lee, H. J.; Jana, J.; Ngo, Y. T.; Wang, L. L.; Chung, J. S.; Hur, S. H. The e Ff Ect of Solvent Polarity on Emission Properties of Carbon Dots and Their Uses in Colorimetric Sensors for Water and Humidity. *Mater. Res. Bull.* **2019**, *119*, No. 110564.
(40) Roshni, V.; Misra, S.; Santra, M. K.; Ottoor, D. One Pot Green Synthesis of C-Dots from Groundnuts and Its Application as Cr(VI) Sensor and in Vitro Bioimaging Agent. *J. Photochem. Photobiol., A* **2019**, *373*, 28−36.
(41) Zhou, X.; Zhao, G.; Tan, X.; Qian, X.; Zhang, T.; Gui, J.; Yang, L.; Xie, X. Nitrogen-Doped Carbon Dots with High Quantum Yield for Colorimetric and Fluorometric Detection of Ferric Ions and in a Fluorescent Ink. *Microchim. Acta* **2019**, *186* (2), 67.
(42) Zheng, M.; Xie, Z. A Carbon Dots−Based Nanoprobe for Intracellular Fe3+ Detection. *Mater. Today Chem.* **2019**, *13*, 121−127.
(43) Ren, G.; Tang, M.; Chai, F.; Wu, H. One-Pot Synthesis of Highly Fluorescent Carbon Dots from Spinach and Multipurpose Applications. *Eur. J. Inorg. Chem.* **2018**, *2018* (2), 153−158.
(44) Li, L.; Zhang, R.; Lu, C.; Sun, J.; Wang, L.; Qu, B.; Li, T.; Liu, Y.; Li, S. In Situ Synthesis of NIR-Light Emitting Carbon Dots Derived from Spinach for Bio-Imaging Applications. *J. Mater. Chem. B* **2017**, *5* (35), 7328−7334.
(45) Chen, M.; Liu, C.; An, Y.; Li, Y.; Zheng, Y.; Tian, H.; Shi, R.; He, X.; Lin, X. Red, Green, and Blue Light-Emitting Carbon Dots Prepared from Gallic Acid for White Light-Emitting Diode Applications. *Nanoscale Adv.* **2021**, *4* (1), 14−18.
(46) Zhang, H.; Guo, H.; Li, D.; Zhang, Y.; Zhang, S.; Kang, W.; Liu, C.; Le, W.; Wang, L.; Li, D.; Dai, B. Halogen Doped Graphene Quantum Dots Modulate TDP-43 Phase Separation and Aggregation in the Nucleus. *Nat. Commun.* **2024**, *15* (1), No. 2980.
(47) Guo, H.; Lu, Y.; Lei, Z.; Bao, H.; Zhang, M.; Wang, Z.; Guan, C.; Tang, B.; Liu, Z.; Wang, L. Machine Learning-Guided Realization of Full-Color High-Quantum-Yield Carbon Quantum Dots. *Nat. Commun.* **2024**, *15* (1), No. 4843.
(48) Bhattacharya, T.; Joshi, R.; Tufa, L. T.; Goddati, M.; Lee, J.; Tewari, A.; Cho, B.-K. L-Cysteine-Modified Carbon Dots Derived from Hibiscus Rosa-Sinensis for Thiram Pesticides Identification on Edible Perilla Leaves. *ACS Omega* **2024**, *9* (48), 47647−47660, DOI: 10.1021/acsomega.4c07090.
(49) Ni, Q.; Zhang, S.; Wang, K.; Guo, H.; Zhang, J.; Wu, M.; Wang, L. Carbon Quantum Dot-Mediated Binary Metal−Organic Framework Nanosheets for Efficient Oxygen Evolution at Ampere-Level Current Densities in Proton Exchange Membrane Electrolyzers. *J. Mater. Chem. A* **2024**, *12* (45), 31253−31261.
(50) Wu, Q.; Wang, X.; Rasaki, S. A.; Thomas, T.; Wang, C.; Zhang, C.; Yang, M. Yellow-Emitting Carbon-Dots-Impregnated Carboxy Methyl Cellulose/Poly-Vinyl-Alcohol and Chitosan: Stable, Free-standing, Enhanced-Quenching Cu2+-Ions Sensor. *J. Mater. Chem. C* **2018**, *6* (16), 4508−4515.
(51) Yang, H.; Liu, Y.; Guo, Z.; Lei, B.; Zhuang, J.; Zhang, X.; Liu, Z.; Hu, C. Hydrophobic Carbon Dots with Blue Dispersed Emission and Red Aggregation-Induced Emission. *Nat. Commun.* **2019**, *10* (1), 1789.
(52) Liu, Y.; Zhou, Q.; Li, J.; Lei, M.; Yan, X. Selective and Sensitive Chemosensor for Lead Ions Using Fluorescent Carbon Dots Prepared from Chocolate by One-Step Hydrothermal Method. *Sens. Actuators, B* **2016**, *237*, 597−604.
(53) Liu, Y.; Zhou, Q.; Yuan, Y.; Wu, Y. Hydrothermal Synthesis of Fluorescent Carbon Dots from Sodium Citrate and Polyacrylamide and Their Highly Selective Detection of Lead and Pyrophosphate. *Carbon* **2017**, *115*, 550−560.
(54) Kim, Y.; Kim, J. Bioinspired Thiol Functionalized Carbon Dots for Rapid Detection of Lead (II) Ions in Human Serum. *Opt. Mater.* **2020**, *99*, No. 109514.
(55) Chauhan, P.; Chaudhary, S.; Kumar, R. Biogenic Approach for Fabricating Biocompatible Carbon Dots and Their Application in Colorimetric and Fluorometric Sensing of Lead Ion. *J. Cleaner Prod.* **2021**, *279*, No. 123639.


https://doi.org/10.1021/acsomega.4c10796
*ACS Omega* 2025, 10, 2354−2363